

Analysis and interpretation of tsunami damage caused by the 2011 Japan earthquake using ENVISAT ASAR images

Yanmei Zhang¹, Zaisen Jiang¹, Ying Fang¹, Xiao Cheng²

¹ Institute of Earthquake Science, China Earthquake Administration, Beijing, 100036, CHINA

² College of Global Change and Earth System Science, Beijing Normal University, Beijing, 100875, CHINA

E-mail: xcheng@bnu.edu.cn

Abstract. An analysis of the ENVISAT advanced synthetic aperture radar (ASAR) observations of the area hit by the 2011 Japan tsunami is presented. The height of the tsunami waves was sufficient to cause widespread inundation of coastal areas. The SAR acquisitions were performed on February 19 (20 days before the tsunami) and March 21 (ten days after the tsunami) in interferometric mode so that not only the information regarding the intensity of the radar signals but also the complex coherence was used. The interpretation of the available data has allowed researchers to detect flooded areas. Though the post-tsunami acquisition is a bit late for the fixed 30-day observation cycle of ENVISAT ASAR sensor, and the spatial resolution of ASAR is relatively low, valuable information regarding the damage was still retrieved. These interpretations have been validated by a series of optical images, which served as benchmarks.

1. Introduction

The 2011 earthquake off the Pacific coast of Tōhoku, also known as the 2011 Tohoku earthquake or the Great East Japan Earthquake, was a magnitude 9.0 (M_w) undersea megathrust earthquake off the coast of Japan. It occurred at 14:46 JST (05:46 UTC) on Friday, March 11, 2011. Its epicenter was approximately 70 km (43 mi) east of the Oshika Peninsula of Tōhoku, and the hypocenter had an underwater depth of approximately 32 km (20 mi), as shown in figure 1. It was the most powerful earthquake ever known to have hit Japan and one of the five most powerful earthquakes recorded anywhere in the world since modern record-keeping began in 1900. The earthquake triggered powerful tsunami waves that reached heights of 40.5 meters (133 ft) in Miyako in Tōhoku's Iwate Prefecture, and which, in the Sendai area, travelled up to 10 km (6 mi) inland. The tsunami caused a number of nuclear accidents [1]. The damage caused by the heavy tsunami was monumental in scale and difficult to estimate.

Satellite remote sensing data are fundamental to evaluating areas involved in natural disasters because of their synoptic view. This approach was particularly effective for this tsunami event, which affected a very large area, making the extensive field survey unfeasible. Radiation emitted from the damaged nuclear reactors made *in situ* investigations dangerous. For these reasons, satellite remote sensing was not only the most effective but also the safest and, to some extent, a unique way of assessing Japan's tsunami-affected areas. Synthetic aperture radar (SAR) data are also particularly



valuable because of their all-weather capability and their specific sensitivity to different kinds of surface changes.



Figure 1. Map showing the epicenter of the M9.0 Sendai earthquake, March 11, 2011.

The Geospatial Information Authority of Japan produced orthorectified aerial photomaps of the disaster area and provided a tsunami inundation map right after the disaster [2]. Miyagi *et al.* and Ozawa used an interferometry technique with PALSAR data and detected crustal movement caused by the earthquake [3, 4]. Approximately 6 cm of crustal movement was observed throughout the Ishinomaki area. Using both the phased array type L-band synthetic aperture radar (PALSAR) and polarimetric and interferometric airborne synthetic aperture radar (PiSAR) full-polarimetric data, Watanabe *et al.* calculated representative polarimetric parameters for urban areas [5]. In these areas, most of the buildings were destroyed by the subsequent tsunami. Gong *et al.* estimated the area affected by tsunami using China's HJ-1 imagery [6]. This imagery was acquired on March 14 based on a normalized difference water index (NDWI). The new Italian satellite SAR sensor, COSMO-SkyMed (CSK) SAR, showed a strong capability for high resolution and short repeat intervals. Acquisitions made in interferometric mode on March 12 and 13, 2011 indicated the locations of the flooded areas and the receding floodwater and even the presence of the debris floating above the surface of the water [7]. SAR images from the TerraSAR-X satellite have also been used to generate a ground motion map by means of correlation techniques and absolute displacements in the radar line of sight and in the satellite flight direction are determined with a divergence of about 15 cm [8].

Launched in 2002, the ENVISAT Advanced Synthetic Aperture Radar (ASAR) system has been successfully used in the management of many disasters, including the Indonesian earthquake and tsunami of 2004 [9]. The ASAR is an advanced instrument that employs a number of new technological developments. The resulting improvements include its ability to provide swath coverage more than 400 km wide and its alternating polarization feature, which allows scenes to be imaged in vertical (V) and horizontal (H) polarizations simultaneously. When in image mode, the ASAR gathers data from relatively narrow swaths (nearly 100 km within a viewing area of approximately 485 km) and high spatial resolution (30 m).

In the present paper, an analysis of pre-tsunami and post-tsunami image mode ASAR images was performed to evaluate the damage done to coastal areas by the tsunami.

2. Data and methods

The present study was performed on ASAR data acquired on February 19 (20 days before the tsunami) and March 21, 2011 (10 days after the tsunami), both at 00:40 UTC. The data covers Sendai and its surroundings, which are close to the epicenter of the seismic event. These areas were heavily affected by the tsunami. These two SAR images were acquired with the same acquisition parameters (as an

interferometric pair) at image mode (nominal resolution: 12 m), horizontal polarization, descending orbit, right looking, and with an incidence angle of 40°. These data were downloaded from the GEO's Tohoku-oki Event Supersite Website (<http://supersites.earthobservations.org>).

The synthetic aperture radar (SAR) backscatter coefficient (σ_0) is a complex function of local characteristics, including topography, geological composition, soil moisture and salinity, and vegetation density and structure. In the case of the tsunami inundation, changes in land cover class take place alongside damage to buildings, flooded areas, and stressed vegetation.

Many different SAR backscattering behaviors can be classified: 1) Low radar return from smooth open water bodies that act as specular reflectors. 2) Double-bounce mechanisms involving the surface of the water beneath the vegetation such that stems and tree trunks enhance backscattering, causing flooded vegetation to appear very bright in a SAR image. 3) Decrease in the backscattering of urbanized damaged areas, where the double-bounce facade soil is lacking [10–12].

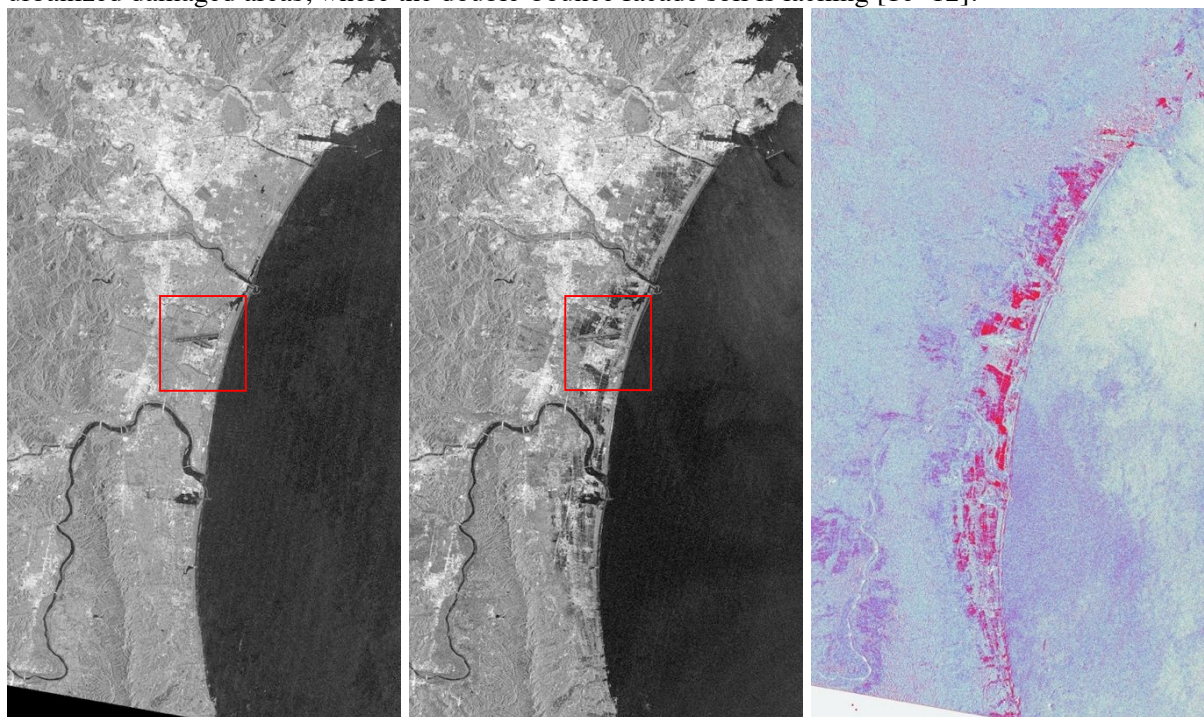


Figure 2. Calibrated and geo-referenced Envisat ASAR σ_0 images of the Sendai region acquired on Feb 9 (left) and Mar 21 (mid). Inundated areas appear dark along the coast. These areas are clearly visible in the middle panel. A differential image is shown in the right panel using ENVI's color-mapping scheme. Regions with significant differences appear red. The red rectangle indicates Sendai Airport and its vicinity.

Single look complex (SLC) format data were calibrated and geocoded by means of the ESA NEST (Next ESA SAR Toolbox) software and used to derive the backscattering coefficient. For this purpose, the latest auxiliary XCA file was used to remove the original antenna pattern and apply the updated one. The following corrections were made: incidence angle, absolute calibration constant, range spreading loss and antenna pattern gain. The output of calibration is σ_0 image was saved in dB. The σ_0 product was then applied to the precise orbit data downloaded from ESA website. However minor misplacements (about 1-2 pixel) between the two images remained.

After the reprojection operation (into UTM 54 region) by NEST, the data were co-registered and then subset to the common and interested region using RSI ENVI 4.7 software. The overlapping portion of the two scenes, including the coastal Sendai region, is shown in figure 2. Because these two images were taken only 30 days apart, they look quite similar, especially in the regions of urban, rivers

and lakes. The main differences were in the coastal region, where the inundated land was clearly visible as a dark area in along the coast.

The differential σ_0 image generated from the two registered σ_0 images is shown in the right panel of figure 2. In order to show the difference, color-mapping scheme provided by RSI ENVI was used to enhance visibility. Significant values appeared red in the image and they reflected the inundated places in the middle image reasonably well. The results showed that the method of σ_0 differencing is valid for this purpose.

The rectangle in figure 2 is enlarged in figure 3 so that the difference in σ_0 before and after the tsunami can be evaluated.

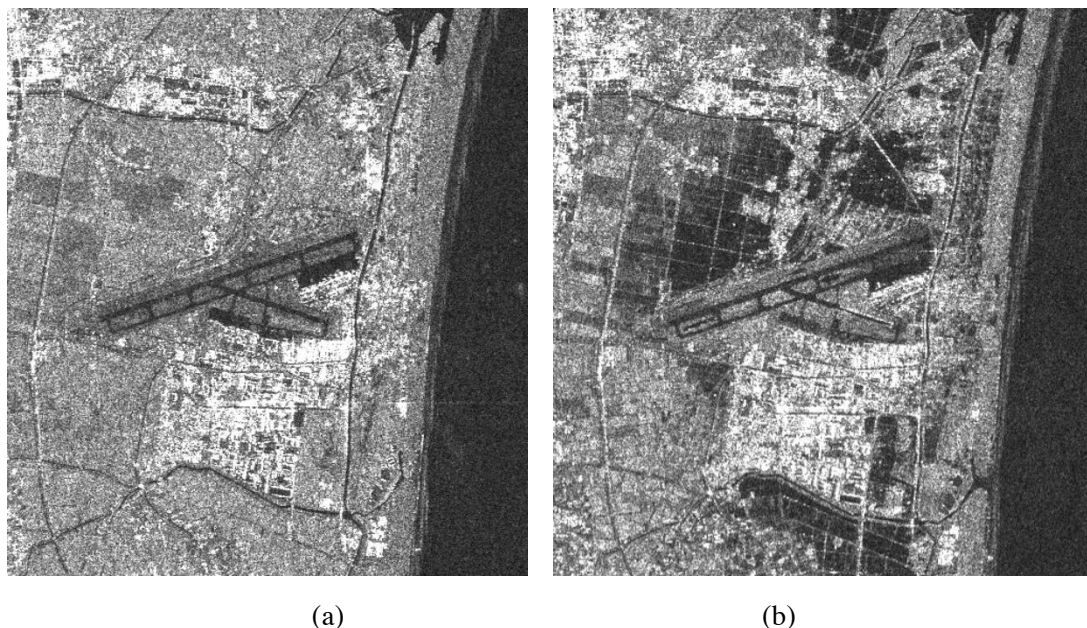


Figure 3. σ_0 image of Sendai Airport and surroundings (left: 20110219, right: 20110321).

In both images of figure 3, the airport runway appears dark because of its specular reflection to radar signal. Settlements south of the airport appear bright because of the corner reflection effect. In figure 3(b), the farmland north of the runway appears dark and shows clear boundaries for different fields. The areas south of the airport appear brighter after the tsunami, which might be because of the collapsed buildings and debris left by the receding water. As shown in figure 3, the areas inundated in this region reached an average of about 5.5 km inland.

The interferometric pair was processed to derive the complex interferogram and coherence using the Gamma ISP software module. An ASTER GDEM v2 (global digital elevation model) with 30 meter postings was introduced for this purpose. ASTER GDEM was generated using stereo-pair images collected by the ASTER instrument onboard the Terra satellite, covering spans from 83° north latitude to 83° south, encompassing 99% of Earth's landmass.

This data pair was also combined for interferometry. The perpendicular component of the baseline was around 180 m and the height ambiguity was about 54 m, accordingly.

The geo-rectified interferogram and coherence images superimposed on the multi-looked SAR intensity image are shown in figure 4. There still exist residual phase errors in the interferogram, induced by the baseline error or by DEM error of the rugged mountain areas.

Those areas showed clear fringes in the left image, corresponding to high-correlation areas. These appear yellow or light purple in the image on the right. There were hardly any visible fringes at those low-correlation tsunami-inundated coastal regions. However, the low-coherence area was a bit larger than the low-backscattering area, which better indicates the flooded and damaged areas.

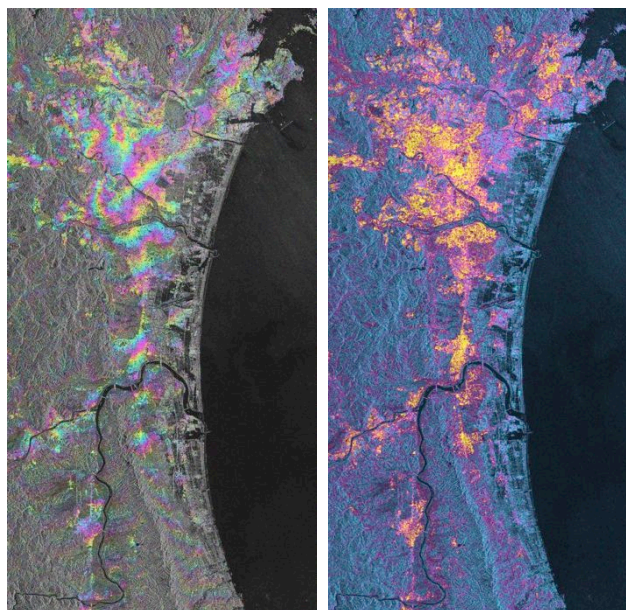


Figure 4. Complex interferogram and coherence image of the interferometric data pair (Master: 20110219; Slave: 20110321). SAR intensity image 20110321 was used as the background. Color-mapping schemes in GAMMA software were used to illustrate the values.



Figure 5. Time-series high-resolution optical images of the Sendai airport region. (UL: 20110314; UR: 20110317; LL: 20110324; LR: 20110327) (Courtesy of Google Earth)

3. Analysis and discussion

In order to study the receding of the tsunami-induced floodwater, a time-series of optical images of the inundated Sendai airport region were collected for comparison. These are shown in figure 5. These images were taken from Google Earth.

As shown in figure 5, the flood receded gradually. On March 14, the whole area was almost completely inundated and on March 17, the water was barely visible in low-lying areas. On March 24, it was difficult to see any water in this area, though the land still appeared wet. In the data collected on March 27, the land surface appeared dry and hardly any floodwater was visible.

The images taken from the shortest distance images are most valid for flood detection. However the acquisition of optical images is always affected by cloud cover, which limits their usefulness. On March 12, this area was covered by thick clouds, which make image acquisition impossible.

The derived tsunami-inundated results in two previous studies were combined [6, 7]. These studies were quite similar to the present study, though they covered a slightly smaller area. The comparison showed that the data and methods used here are successful for this type of application. These results indicated that ASAR imaging remains effective even 10 days after a flood. This is because of the increase in soil moisture of the flood area. However, for regions with impervious surfaces, which recover shortly after floods, surface characteristics and interferometric correlations usually remain constant and cause this method to fail.

Even with the emergence of advanced SAR sensors with higher spatial resolution and shorter revisit intervals, such as ALOS PALSAR, COSMO-SKYMED, and TerraSAR-X, ENVISAT ASAR with its revised 30 d revisit interval still shows a powerful ability to detect tsunami-induced floods. It was used to assess the 2011 Tohoku earthquake during its 10th year of operation. Because the ENVISAT mission ended on April 8, 2012, the scientific community now looks forward to the launch of ESA's Sentinel-3 in April 2014.

Acknowledgements

This work was supported by China's National Science and Technology Support Program (2012BAK19B01-06) and National Natural Science Foundation of China (Grant No. 41274098). The authors would like to thank the GEO's Tohoku-oki Event Supersite Website for providing the ENVISAT ASAR data and Google Earth for providing high-resolution optical images, which were here used as benchmarks.

References

- [1] http://en.wikipedia.org/wiki/2011_Tohoku_earthquake_and_tsunami
- [2] Geospatial Information Authority of Japan. [On-line]. Available: <http://www.gsi.go.jp/>
- [3] Miyagi Y, Takahashi M and Shimada M 2011 *Japan Geoscience Union Meeting*
- [4] Ozawa S, Nishimura T, Suito H, Kobayashi T, Tobita M and Imakiire T 2011 Coseismic and postseismic slip of the 2011 magnitude-9 Tohoku-Oki earthquake *Nature* **475** 373-376
- [5] Watanabe M, Motohka T, Miyagi Y, Yonezawa C and Shimada M 2012 *IEEE Geosci. and Remote Sens. Lett.* **9** 472-476
- [6] Gong P, Zhang H, Zhang H, Liang L and Wang L 2011 *J. Remote Sens.* **15** 863-865
- [7] Chini M, Pulvirenti L and Pierdicca N 2012 *IEEE Geosci. and Remote Sens. Lett.* **9** 467-471
- [8] Yague-Martinez N, Eineder M, Cong X and Minet C 2012 *IEEE Geosci. and Remote Sens. Lett.* **9** 539-543
- [9] Bovolo F and Bruzzone L 2007 *IEEE Trans. Geosci. Remote Sens.* **45** 1658-1670
- [10] Stramondo S, Bignami C, Chini M, Pierdicca N and Tertulliani A 2006 *Int. J. Remote Sens.* **27** 4433-4447
- [11] Pierdicca N, Chini M, Pulvirenti L and Macina F 2008 *Sensors* **8** 4151-4164
- [12] Pulvirenti L, Chini M, Pierdicca N, Guerriero L and Ferrazzoli P 2011 *Remote Sens. Environ.* **115** 990-1002